Heliyon 10 (2024) e26281

Contents lists available at ScienceDirect

Heliyon

journal homepage: www.cell.com/heliyon

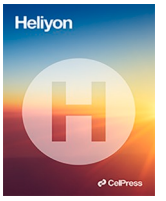

Research article

A comparison between 2D and 3D cobalt–organic framework as catalysts for electrochemical CO_2 reduction

Neda Sadat Barekati [a], Hossein Farsi [a,b,*], Alireza Farrokhi [a], Shokufeh Moghiminia [b]

[a] Department of Chemistry, University of Birjand, Birjand, Iran
[b] DNEP Research Lab, University of Birjand, Birjand, Iran

ARTICLE INFO

Keywords:
Electrochemical CO_2 reduction
Hydrogen evolution
2D MOF
ZIF-67

ABSTRACT

Electrocatalytic CO_2 reduction, as an effective way to reduce the CO_2 concentration, has gained attention. In this study, we prepared ZIF-67 nanoparticles and nanosheets and investigated them as electrocatalysts for CO_2 reduction. It was found that ZIF-67 nanosheets, because of their two–dimensional morphologies, provide more under–coordinated cobalt nodes and have lower overpotentials for both hydrogen evolution and CO_2 reduction reactions. Also, the rate–determining step for hydrogen evolution changes from Volmer for ZIF-67 nanoparticles to Hyrovsky for ZIF-67 nanosheets. Also, the presence of Mg^{2+} ions in solution causes more facile CO_2 reduction, especially for ZIF-67 nanosheets.

1. Introduction

It is quite obvious that CO_2 emissions from burning fossil fuels are completely unavoidable, which is at the heart of the problem because it causes serious environmental and human health problems. To overcome these problems, the best approach is to convert CO_2 into hydrocarbon fuels such as methanol and methane as a renewable energy resource because CO_2 is a futuristic source of C1 feedstock for the production of fuels and value–added chemicals [1–3]. Electrochemical CO_2 reduction reaction (CO_2RR) has received great interest recently, not only for decreasing CO_2 accumulation, as it could be a good process to produce valuable fuels with high energy density [4,5]. Metallic catalysts such as Au, Ag, Pd, and Zn are charming for electrochemical CO_2 reduction due to their excellent catalytic activity and selectivity, but it is practically impossible to use them on a large scale due to their scarcity and high price [6,7]. So far, many attempts have been made to design and synthesize efficient electrocatalysts for CO_2 reduction. However, despite many efforts, the high overpotential, poor product selectivity, and low Faradaic efficiency are still significant hurdles for further development of CO_2RRs because much energy is required to reduce CO_2 molecules, which have a thermodynamically stable structure [8,9].

Metal–organic frameworks (MOFs) are formed by connecting metal ions and organic linkers through covalent coordination linkages [10,11]. MOFs have attracted much attention due to their attractive properties, such as tunable pore size, high porosity, high specific surface area, regular structure, and open metal sites [12,13]. On the other hand, due to the various types of catalytic sites present in the MOFs, they can provide the inherent advantages of both homogeneous and heterogeneous catalysts [14–17]. In addition, in the field of electrocatalysis, MOFs have been reported as effective electrocatalysts for overall water splitting and CO_2 reduction reactions because these materials contain both organic and inorganic sources [18–20]. Despite all the benefits listed above, some inherent shortcomings in these compounds cannot be ignored, such as conductivity, which leads to a significant reduction in the

* Corresponding author. Department of Chemistry, University of Birjand, Birjand, Iran.
E-mail address: hofarsi@birjand.ac.ir (H. Farsi).

https://doi.org/10.1016/j.heliyon.2024.e26281
Received 11 October 2023; Received in revised form 1 February 2024; Accepted 9 February 2024
Available online 10 February 2024
2405-8440/© 2024 The Authors. Published by Elsevier Ltd. This is an open access article under the CC BY-NC-ND license (http://creativecommons.org/licenses/by-nc-nd/4.0/).

electrochemical applications of these compounds [21–23]. Fortunately, ultrathin two–dimensional (2D) MOF nanosheets (NSs) have attracted much attention in the field of electrocatalysis because of their crystalline structure, microporosity, conductivity, and abundance of exposed active sites [24–28]. Therefore, it is crystal clear that the 2D MOF NSs have the positive points of both MOFs and 2D nanomaterials and eliminate the negative points of MOFs [29]. In this regard, today we witness the widespread electrochemical applications of 2D MOF NSs in a wide variety of fields, especially in electrochemical CO_2RR [30]. In the previous studies, several 2D MOF catalysts acquired excellent electrocatalytic performance for electrochemical CO_2RR, such as ultrathin 2D nickel (II) ZIF NSs [31] and ultrathin 2D MOF NSs [TCPP(Co)/Zr–BTB] [32].

On the other hand, it has been shown that the concentration of Mg^{2+} ions in the stroma has an important role in CO_2 fixation by chlorophyll [33,34]. Also, the addition of Lewis acid cations such as Mg^{2+} ions to the electrolyte improves the catalytic behavior of cobalt phthalocyanine [35] and iron porphyrins [36,37] by the formation of a complex containing Mg^{2+} and CO_2. Due to these observations, researchers have investigated MOFs containing Mg metallic centers, such as Mg-MOF-74 [38] and Mg–centered porphyrin MOF [39]. In this study, for the first time, we have investigated the CO_2 electrochemical reduction in the solution containing Mg^{2+} ions on the surface of zeolitic imidazolate framework-67 (ZIF-67), believing the unsaturated metallic nodes in ZIF-67 can make a complex called ZIF-67-CO_2-Mg^{2+} with the similar approach used by Wang et al. for cobalt–phthalocyanine molecules [35].

In this work, we synthesized ZIF-67 as an electrocatalyst for electrochemical CO_2 reduction. ZIF-67 is formed by bridging cobalt cations and 2–methylimidazolate anions with a pore size of about 0.34 nm, although, because of its flexible structure, the pore size may reach 0.4–0.45 nm values [40]. Based on the kinetic diameters of CO_2 gas molecules (0.33 nm), the presence of these pores can affect the exceptional selective capture and storage of CO_2 gas molecules [41]. This is a smart choice for two reasons: 1) Due to its appropriate pore size and selective adsorption abilities of CO_2, ZIF-67 is an ideal candidate for electrochemical reduction of CO_2 because the CO_2 absorption on the electrode surface is very considerable, since the absorption of CO_2 on the electrode surface can reduce the activation energy of the electrochemical reduction [42]. 2) Cobalt is an earth–abundant metal and less expensive than noble metals, which form compounds with different valence states [43]. Additionally, herein we report an impressive method of morphology regulation to ameliorate the electrocatalytic performance of ZIF-67 without post–treatment. First, we synthesized ultrathin 2D ZIF-67 NSs from a mixed solution of 2–methylimidazole and cobalt using a controllable one–pot hydrothermal preparation strategy. Second, three–dimensional (3D) ZIF-67 nanoparticles (NPs) were successfully synthesized at room temperature (25 °C) in distilled water, which is environmentally friendly. Eventually, we observed that the ultrathin 2D ZIF-67 NSs represent a lower onset potential and superior electrocatalytic activity towards electrochemical CO_2 reduction in alkaline solution and both in the presence and absence of Mg^{2+} ions in $NaHCO_3$ solution because the unsaturated cobalt active centers on the surface of ultrathin 2D ZIF-67 NSs could significantly elevate the electrochemical catalysis performance, which is enhanced in the presence of Mg^{2+} ions due to ZIF-67 CO_2–Mg^{2+} complex formation.

2. Experimental section

2.1. Materials

All solvents and reagents studied were of analytical grade and used without further purification. All chemicals, 2–methylimidazole ($C_4H_6N_2$, 99%), cobalt (II) nitrate hexahydrate ($Co(NO_3)_2{\cdot}6H_2O$, 98%), N, N–dimethylformamide (C_3H_7NO, 99.8%), ethanol (CH_3CH_2OH, 99.8%), and methanol (CH_3OH, 99.8%), were purchased from Sigma–Aldrich. All aqueous solutions were prepared using high–purity deionized water (DI–water, resistance 18 MΩ cm^{-1}).

2.2. Synthesis of ZIF-67 nanoparticles and nanosheets

For ZIF-67 nanoparticles, a solution of 2–methylimidazole (133.98 mmol, 11.00 g) in 45 mL deionized water was added to a solution of $Co(NO_3)_2{\cdot}6H_2O$ (3.10 mmol, 0.90 g) in 10 mL deionized water and vigorously stirred for 7 h at 25 °C. The purple–colored precipitate was separated by centrifugation, washed with water, and dried at 25 °C for 72 h. The schematic of the synthesis procedure is

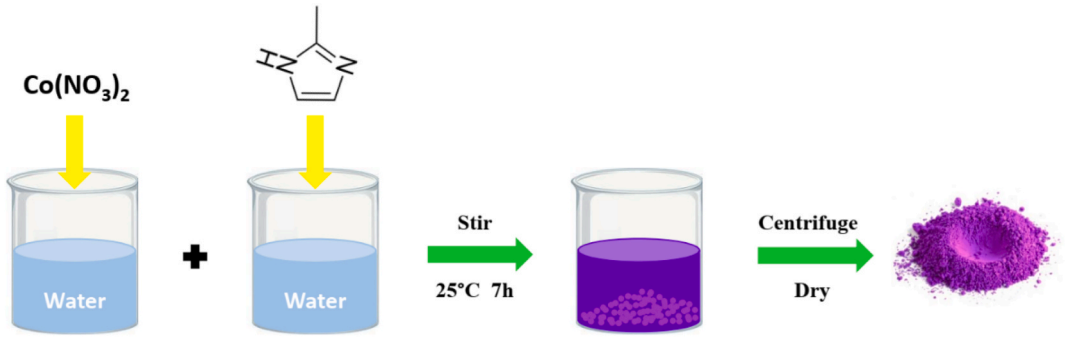

Fig. 1. The schematic of the synthesis procedure for ZIF-67 nanoparticles using the coprecipitation method.

displayed in Fig. 1.

For the synthesis of ZIF-67 nanosheets, 3.44 mmol of $Co(NO_3)_2{\cdot}6H_2O$ was dissolved in a mixed solution of 30 mL of deionized water, 30 mL of ethanol, and 30 mL of DMF under stirring. Then, 6.10 mmol of 2–methylimidazole was added to the above solution. After the complete dissolution of 2–methylimidazole, the mixture solution was immediately transferred into a Teflon–lined stainless steel autoclave with a 200 mL capacity. Subsequently, the autoclave was kept in an oven at 160 °C for 12 h. Finally, the obtained samples were washed using methanol to remove the impurities and dried at 100 °C in a vacuum for 12 h. Fig. 2 illustrates the schematic of the synthesis of ZIF-67 nanosheets.

2.3. Material characterization

Powder X–ray diffraction (XRD) patterns were obtained for synthesized samples using a Rigaku Ultima IV diffractometer equipped with a Cu Kα source (λ = 1.5406 Å). Field emission scanning electron microscopy (FE–SEM, Mira3 TESCAN–XMU) was used for examining the morphology of the samples. An atomic force microscope (AFM) instrument (Bruker Dimension Icon) was employed to examine the size and thickness of the ZIF-67 NSs. To investigate the surface area and pore size distribution, Brunauer–Emmett–Teller (BET) and Barrett–Joyner–Halenda (BJH) were tested on Belsorp Mini II.

2.4. Electrochemical measurement

The thin film working electrodes were designed precisely the same as the prior electrodes by the electrophoretic deposition method [44–46]. All the electrochemical measurements were performed at 25 °C by a conventional three–electrode cell, with a saturated Ag/AgCl as the reference electrode, an electrophoretically deposited material electrode as the working electrode, and a platinum grid as the counter electrode in an aqueous 1.0 M KOH electrolyte solution. The electrolytes for investigation of the effects of the presence of Mg^{2+} ions were considered as 0.1 M $NaHCO_3$ + 0.05 M NaCl and 0.1 M $NaHCO_3$ + 0.05 M $MgCl_2$ solutions, similar to Wang et al.'s report [35], unless here we used chloride salts instead of their chlorate salts. Linear sweep voltammetry was carried out with the Solartron Electrochemical Interface SI 1287.

3. Results and discussions

The ZIF-67 NP has been synthesized at room temperature without the presence of any toxic solvent, which can be very beneficial for the production of MOFs on an industrial scale. The ZIF-67 NS is synthesized by a one–pot hydrothermal method; the most important advantage of this method is that it does not use any surfactant molecules.

The crystal structure of the as–prepared samples was examined by XRD. The powder XRD pattern of ZIF-67 NP is collected in Fig. 3 (A). It can be seen that the XRD pattern of the ZIF-67 NP sample is completely consistent with the simulated data from Jeong et al. [47], and no additional peaks are observed, which indicates the purity and the successful synthesis of the sample. As shown in Fig. 3(C), the XRD pattern of the ZIF-67 NS exhibits only first and second reflections from (211) and (422) crystallographic planes, emphasizing crystal growth under our synthetic conditions, which is restricted to these crystalline facets. This is quite obvious because, due to the measures adopted in the synthesis of this sample, it is expected that we will see growth limitations [48]. In Fig. 3(B) and (D), we have presented the crystal structures of ZIF-67 NP and ZIF-67 NS simulated using the CIF file of ZIF-67 [47] and Mercury 4.0 Software, respectively.

The morphology of both samples was characterized by FE–SEM analysis. Fig. 4 displays the FE–SEM images of the samples. As shown in Fig. 4(A) and (B), the prepared ZIF-67 NP illustrates a smooth surface with a rhombic dodecahedral shape. Fig. 4(C) and (D) demonstrate the FE–SEM images of the ZIF-67 NS, where the stacked nanosheets–like morphology of the sample is clearly visible.

The AFM analysis was used to assess the flake morphology and estimate the thickness of the single nanosheet. Based on the AFM image (Fig. S1), the thickness of ZIF-67 NS is smaller than 2 nm, which confirms the sheet morphology of the prepared ZIF-67 NS.

The N_2 adsorption–desorption isotherms were employed to evaluate the porosity and surface area of the obtained MOFs. As shown in Fig. 5(A)–a typical type–I isotherm with an H_4–type hysteresis loop was observed for the ZIF-67 NP, which is characteristic of

Fig. 2. The schematic of the synthesis procedure for ZIF-67 nanosheets via the hydrothermal method.

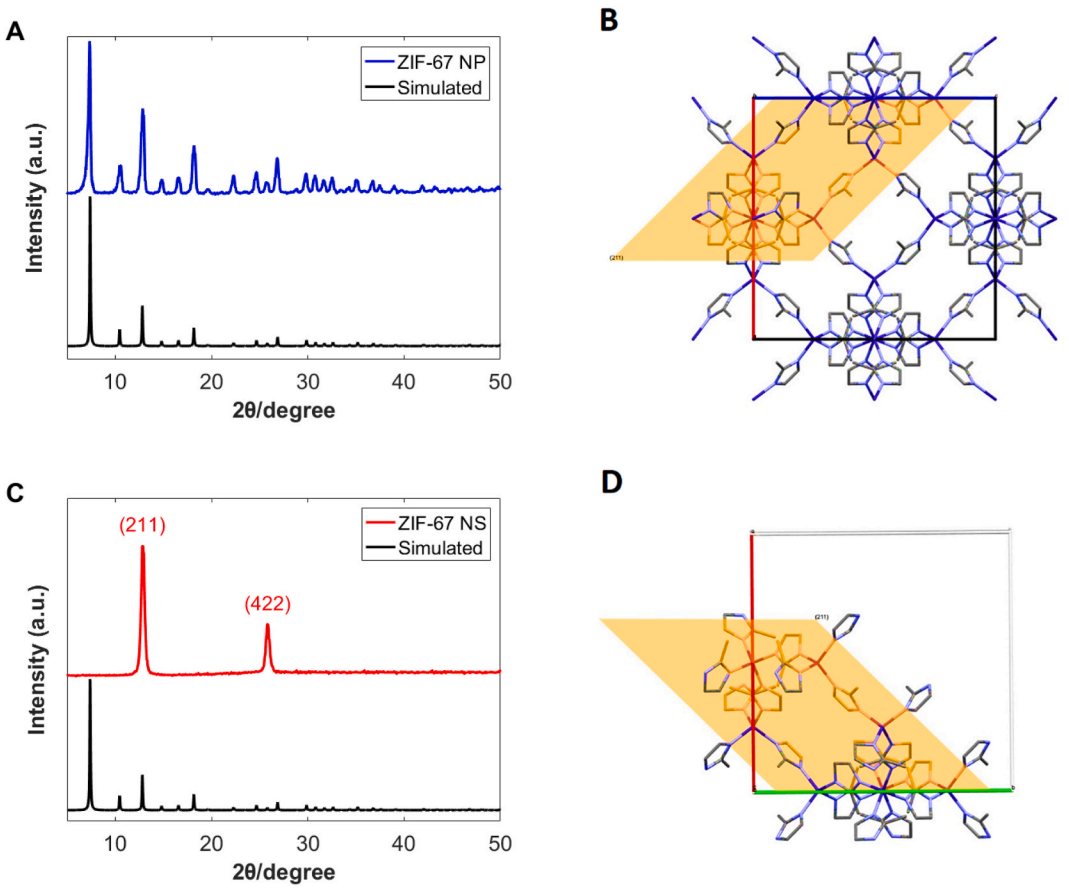

Fig. 3. (A) Powder XRD patterns of simulated ZIF-67 (JCPDS: 671073) and ZIF-67 NP; (B) the crystal structure of ZIF-67 NP; (C) the XRD patterns of simulated ZIF-67 (JCPDS: 671073) and ZIF-67 NS; and (D) the crystal structure of ZIF-67 NS.

microporous materials [49]. For the ZIF-67 NS sample, we observe the type–III isotherm with an H_3–type hysteresis loop, which proves the confirmation of the layered structure of the sample, as depicted in Fig. 5(B) [50]. The comparison between these isotherms at low pressures shows that a huge amount of N_2 gas is adsorbed on the surface of ZIF-67 NP compared to ZIF-67 NS because of its minimal porosity, and consequently, it will have a much greater contribution of external surface area in electrocatalysis with a smaller specific surface area compared to ZIF-67 NP [51]. This argument is verified by experimentally specific surface area determination, which shows ZIF-67 NP and ZIF-67 NS have BET surface areas of 953 and 127 $m^2\ g^{-1}$, respectively. The detailed textural parameters of both samples are listed in Table 1.

After the characterization of the prepared samples, they were investigated for electrochemical reduction of CO_2, a process that happens in negative potentials where cobalt nodes in ZIF-67 have already been reduced in alkaline solution via [52]:

$$Co(OH)_2(s) + 2e^- \leftrightarrows Co(s) + 2OH^- \quad (E_0 = -0.73\ V) \tag{1}$$

The hydrogen evolution reaction (HER) is a competitor reaction for the CO_2 reduction reaction [53]. Cobalt compounds have illustrated good activity towards HER and introduced a metallic cobalt center as the active site for HER, although the atmosphere around this center has an important role in accelerating water molecule adsorption as well as the desorption of intermediates in HER [43,54–57]. Also, it has been shown that the active site for CO_2 reduction is cobalt atoms in cobalt–based electrocatalysts, which, with a nucleophilic attack, activate CO_2 molecules [58–60]. Therefore, we expect competition between H_2O and CO_2 molecules to be adsorbed on the surface of cobalt nodes. We used linear sweep voltammetry (LSV) to investigate this competition. We took the LSVs before and after bubbling the 1.0 M KOH solution with CO_2 for both ZIF-67 NP and ZIF-67 NS electrodes.

CO_2 bubbling in alkaline solutions causes a decrease in the pH of these solutions because CO_2 in alkaline solutions participates in hydrolysis equilibriums:

$$CO_2(g) + OH^-(aq) \rightleftarrows HCO_3^- \tag{2}$$

$$HCO_3^-(aq) + OH^-(aq) \rightleftarrows CO_3^{2-}(aq) \tag{3}$$

So different carbonaceous species (HCO_3^-, CO_2, CO_3^{2-}) exist in the solution. The major species are dependent on the pH of the

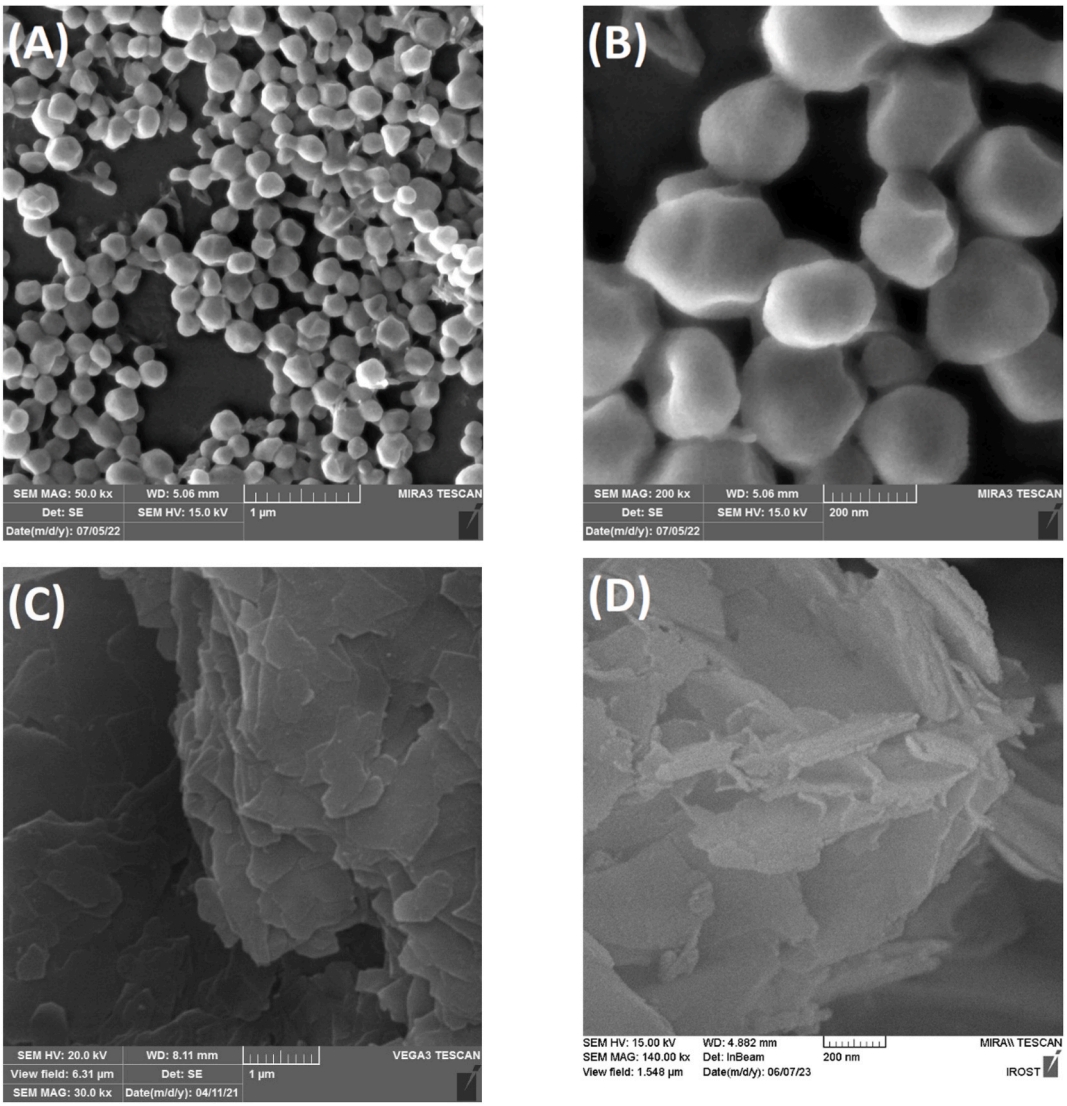

Fig. 4. FE–SEM images of (A) and (B) ZIF-67 NP, and (C) and (D) ZIF-67 NS with two different magnifications.

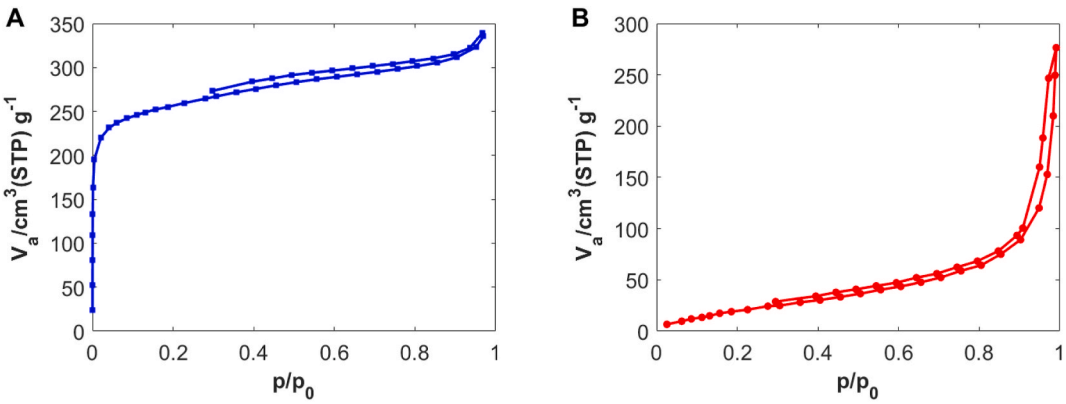

Fig. 5. The N_2 adsorption–desorption isotherms of the prepared (A) ZIF-67 NP and (B) ZIF-67 NS.

Table 1
Results of the BET analysis for ZIF-67 NP and ZIF-67 NS.

Samples	BET surface area ($m^2\ g^{-1}$)	Mean pore diameter (nm)	Total pore volume ($cm^3\ g^{-1}$)
ZIF-67 NP	953	1.21	0.36
ZIF-67 NS	127	1.18	0.33

electrolyte. The pH of 1.0 M KOH solution reaches 7.0 with CO_2 bubbling, where Fujii et al. reported that the dominant anion is HCO_3^- [61]. Therefore, the solutions have different pHs before and after CO_2 bubbling. To remove the effects of pH on the potentials, we have calculated all potentials versus reversible hydrogen electrode (RHE) using:

$$E_{RHE}(V) = E_{Ag/AgCl} + 0.199 + 0.0592 \times pH \quad (4)$$

Where E_{RHE} and $E_{Ag/AgCl}$ are potentials against reversible hydrogen electrode (RHE) and Ag/AgCl reference electrode, respectively.

Fig. 6(A) and (B) illustrate the existence of CO_2, H_2O, and HCO_3^- around the ZIF-67 NP and ZIF-67 NS, respectively, and competition between H_2O and CO_2 molecules to adsorb on the surface of cobalt atoms. Zheng et al. reported that the existence of HCO_3^- ions in the solutions during electroreduction of CO_2 exhibits a transition from inhibitory to promotional effect by going to higher overvoltage [62], and we used this advantage in all parts of our CO_2 reduction evaluation. Fig. 6(C) depicts linear sweep voltammetry (LSV) curves of HER in the presence and absence of CO_2 bubbling for ZIF-67 NS and ZIF-67 NP in 1.0 M KOH solution at a scan rate of 10 mV s^{-1}. It is obvious that the presence of CO_2 in the solution for both ZIF-67 morphologies exhibits a poisoning effect for HER [53]. This implies that either the CO_2–reduction intermediates blocked adsorptive sites, here cobalt nodes, for hydrogen adsorption, or chemical species in the solution or adsorbed on the surface led to the weakening of the bonding of hydrogen to the surface [63].

To compare the abilities of ZIF-67 NP and ZIF-67 NS towards CO_2 reduction, we have obtained the overpotential values at a current density of 5 mA cm^{-2} (η_5) in the presence and absence of CO_2, using LSVs presented in Fig. 6(C). The obtained results are tabulated and presented in Table 2. Therefore, we witness that the HER in the presence of CO_2 is delayed for both samples and is observed at higher potentials because, first, the CO_2 species are adsorbed on the electrode surface, and after the electrochemical CO_2 reduction reaction, the produced products on the sites due to the high applied potential leave these sites, and then water molecules are adsorbed on these sites, and HER immediately occurs. In fact, such behavior has been reported for the transition metals, which have weak H–binding energy in HER volcano plot such as Cu and Co [63,64]. In the presence of CO_2, onset potential changes from −0.05 to −0.15 V and from

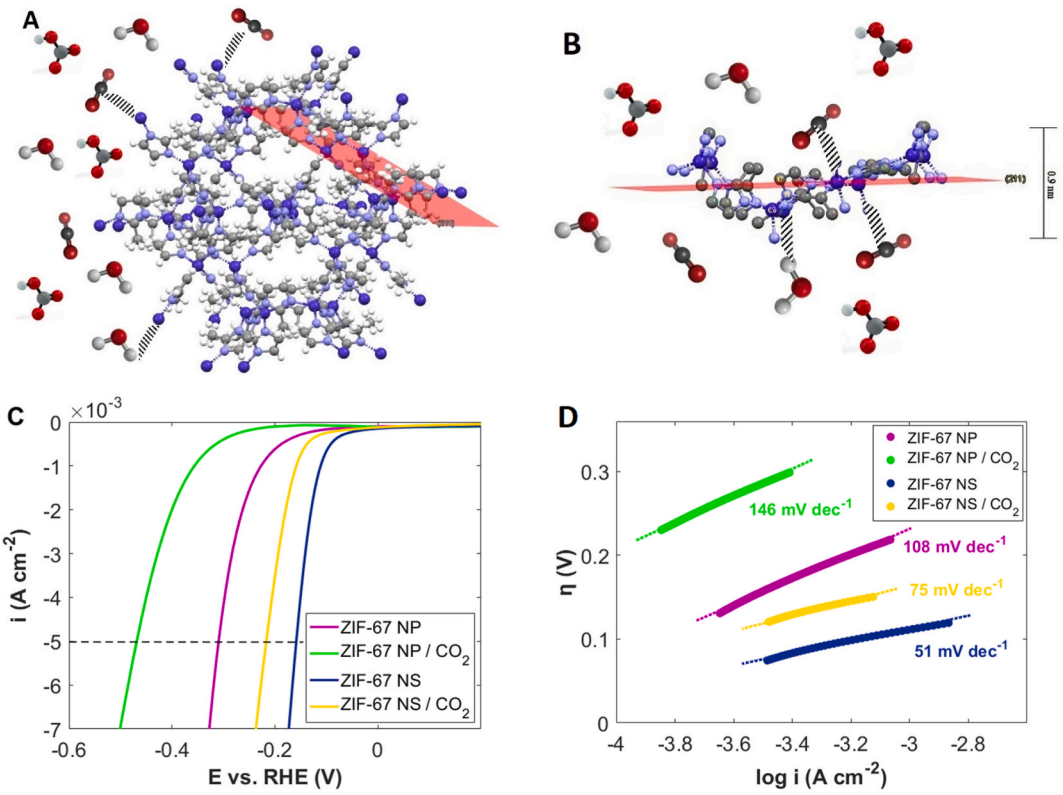

Fig. 6. The competition between CO_2 and H_2O to adsorb on the (A) ZIF-67 NP and (B) ZIF-67 NS in the presence of HCO_3^- ions. (C) LSV and (D) Tafel plot for ZIF-67 NP and ZIF-67 NS in CO_2–saturated and without CO_2 addition at 1.0 M KOH.

Table 2
Overpotentials and Tafel slopes for ZIF-67 NS and ZIF-67 NP.

Samples	Electrolyte	η_5 (V)	Tafel slope (mV dec^{-1})
ZIF-67 NP	1.0 M KOH	0.31	108
	1.0 M KOH + CO_2	0.44	146
ZIF-67 NS	1.0 M KOH	0.16	51
	1.0 M KOH + CO_2	0.22	75

−0.20 to −0.30 V vs. RHE for ZIF-67 NS and ZIF-67 NP, respectively. This trend remains intact at more negative potentials compared to onset potentials [53]. The numerical values show that ZIF-67 NS exhibits lower overpotentials compared to ZIF-67 NP in both with and without CO_2 bubbling conditions. Yang et al. introduced the energy gap between the counter ion p–band and Co d–band centers as an effective descriptor, which is an optimal balance between H–atom adsorption and hydrogen molecule desorption from the surface [56]. In fact, factors such as size and morphology [54,65], counter ion or organic linker [57,66–69], doping, and defect engineering [57] could affect this descriptor. For our case, both samples have the same metallic nodes and organic linker, but the difference between them returns to the contribution of unsaturated cobalt nodes (under–coordinated), which are more activated than the regular cobalt nodes. As we have already mentioned for the interpretation of BET results, ZIF-67 NS has a smaller internal surface area, lower porosity, and a higher external exposure surface area, and consequently, a major contribution of under–coordinate cobalt nodes because of its 2D morphology compared to ZIF-67 NP. Thus, it is expected that the heat of adsorption of hydrogen atoms on the under–coordinate cobalt node will be greater than that of the regular nodes.

The linear part of the polarization curves (Tafel plot) for the HER in the presence and absence of CO_2 in a 1.0 M aqueous KOH solution has been indicated in Fig. 6(D). The ZIF-67 NS displays the lowest Tafel slopes in the presence and absence of CO_2 bubbling at 75 and 51 mV dec^{-1}, respectively. Tafel slopes for ZIF-67 NP were calculated in the presence and absence of CO_2 bubbling at 146 and 108 mV dec^{-1}, respectively.

From the mechanistic viewpoint, the first step in HER is cleaving the O–H bond of adsorbed water molecules [52,70], here on the cobalt nodes of ZIF-67 (Co–ZIF), which is called the Volmer step with a Tafel slope of 120 mV dec^{-1}:

$$H_2O + Co - ZIF + e^- \rightarrow H - Co - ZIF + OH^- \quad (5)$$

and after that, HER occurs either via the reaction between another water molecule with an adsorbed hydrogen atom (Hyrovsky step) with a Tafel slope of 40 mV dec^{-1}:

$$H_2O + H - Co - ZIF + e^- \rightarrow Co - ZIF + H_2 + OH^- \quad (6)$$

or via the reaction between two adsorbed hydrogen atoms (Tafel step) with a Tafel slope of 30 mV dec^{-1}:

$$2H - Co - ZIF \rightarrow 2\,Co - ZIF + H_2 \quad (7)$$

As the reported data in Table 2 illustrates, the Tafel slope values for ZIF-67 NS and ZIF-67 NP are close to the Hyrovsky and Volmer steps, respectively. It means the rate–determining step (RDS) for ZIF-67 NP is bond breaking in adsorbed water molecules, whereas for ZIF-67 NS, breaking the O–H bond of free H_2O, desorption of adsorbed H, and formation of a free H_2 molecule are RDS. As we have already mentioned, in ZIF-67 NS, a greater number of cobalt nodes are under–coordinated and more reactive compared to ZIF-67 NP; consequently, the heat of adsorption assists the reactants to overcome the energy barrier in the Volmer step in the ZIF-67 NS case (see Fig. 6(C) and (D)).

However, because the Tafel slopes are taken around onset potentials in the presence of CO_2, where a competition between HER and CO_2 reduction exists, the CO_2–reduction mechanism should be considered when interpreting the Tafel slope values. The Tafels slopes have been calculated and reported for producing both CO and formate ions via different rate–determining steps [71,72]:

$$* + CO_2(aq) + e^- \rightarrow CO_2^- ads \quad \left(118\ \text{mV dec}^{-1}\right) \quad (8)$$

$$CO_2^- ads + HCO_3^-(aq) + e^- \rightarrow COOH_{ads} + CO_3^{2-}(aq) \quad \left(59\ \text{mV dec}^{-1}\right) \quad (9)$$

$$COOH_{ads} + HCO_3^-(aq) + e^- \rightarrow CO_{ads} + H_2O + CO_3^{2-}(aq) \quad \left(39\ \text{mV dec}^{-1}\right) \quad (10)$$

$$CO_{ads} \rightarrow CO + * \quad \left(30\ \text{mV dec}^{-1}\right) \quad (11)$$

$$CO_2^- ads + HCO_3^-(aq) + e^- \rightarrow OCHO_{ads} + CO_3^{2-}(aq) \quad \left(59\ \text{mV dec}^{-1}\right) \quad (12)$$

$$OCHO_{ads} + e^- \rightarrow HCOO_{ads}^- \quad \left(39\ \text{mV dec}^{-1}\right) \quad (13)$$

$$HCOO_{ads}^- + e^- \rightarrow HCOO^-(aq) \quad \left(30\ \text{mV dec}^{-1}\right) \quad (14)$$

The first step is the common step for producing all CO_2 reduction products. Steps 9–11 have been suggested for CO production, while steps 12–14 have been considered for more stable liquid carbonaceous products, i.e., formate or formic acid. Our determined

Tafel slopes in the presence of CO_2 are 146 and 75 mV dec^{-1} for ZIF-67 NP and ZIF-67 NS, respectively. It means the rate–determining step in CO_2 depends on the morphology of ZIF-67. Regarding its Tafel slope, the rate–determining step for CO_2RR on the surface of ZIF-67 NP is reaction 8. Although the obtained values are larger than the calculated ones, the Tafel slopes of 140 mV dec^{-1} in 0.1 M $NaHCO_3$ [73], 145 mV dec^{-1} in 0.1 M $NaHCO_3$ [74], 141 mV dec^{-1} in 0.5 M $KHCO_3$ [75], 148 mV dec^{-1} in 0.5 M $KHCO_3$ [76], and 143–149 in 0.5 M $KHCO_3$ [77] have been reported for this rate–determining step on the surface of Au, Sn, Au/C, Ag, and Cu, respectively. It is expected that this reaction could be r.d.s. because, with an electrosorption of CO_2 on the surface, the hybrid of carbon changes from sp to sp^2, and the bond angle changes from 180° to 120°, and such changes require a lot of energy. However, a different situation exists for r.d.s. with a Tafel slope of 75 mV dec^{-1} on the surface of ZIF-67 NS. It has been shown that such a Tafel slope could be related to a chemical reaction with a pre–equilibrium one electron transfer reaction as r.d.s. [78–83], i.e.:

$$* + CO_2(aq) + e^- \rightleftarrows CO_2^- ads \tag{15}$$

$$CO_2^- ads + HCO_3^-(aq) + e^- \rightarrow HCOO_{ads} + CO_3^{2-}(aq) \tag{16}$$

Another point is that the difference between overpotentials in the presence and absence of CO_2 at a current density of 5 mV cm^{-2} ($\Delta\eta_5$) for ZIF-67 NS is smaller than that for ZIF-67 NP. Emphasizing the evacuation of occupied reactive sites by CO_2 reduction intermediates for ZIF-67 NS is more facile than ZIF-67 NP. The reason could be the effect of HCO_3^- ion to promote the electroreduction of CO_2, which acts as a proton donor and causes a sequential electron transfer–proton transfer mechanism to become dominant [62]. For both morphologies of ZIF-67, HCO_3^- ion illustrates such behavior in high overpotentials. However, because of the 2D morphology of ZIF-67 NS, diffusion of HCO_3^- ions between the layers is more facile [84,85] compared to inside the pores of ZIF-67 NP, and HCO_3^- ions will be more available for CO_2 reduction intermediates.

Finally, we investigate the effects of the existence of Mg^{2+} cations inside the electrolyte on CO_2 electroreduction. The reductive LSVs have been taken for both samples in two electrolytes: 0.1 M $NaHCO_3$ + 0.1 M NaCl and 0.1 M $NaHCO_3$ + 0.05 M $MgCl_2$ solutions, and the results have been illustrated in Fig. 7(A) and (B) for ZIF-67 NS and ZIF-67 NP, respectively.

As LSVs show, both ZIF-67 morphologies demonstrate noticeable electrocatalytic activity for CO_2 reduction because they exhibit higher reduction currents in the presence of CO_2 in the absence and the presence of Mg^{2+} ions. In comparison with the last part of this work, an interesting point here is that at a current density of 5 mA cm^{-2} in the presence of CO_2, the overpotential is against the previous part of this work. The reason could be the specific adsorption of chloride ions [86]. In fact, it has been reported that halides enhance the CO_2 reduction reaction toward C–C coupling and producing C_2–products such as ethylene and ethanol because, in the presence of such anions, concentrations of adsorbed CO and maybe other CO_2–reduction intermediates increase [87,88], which is verified by the high current reduction peak in the presence of CO_2 observed in potential ranges between −0.1 and −0.4 V vs. RHE in LSVs of Fig. 7(A) and (B). Also, as the LSVs depict, the existence of Mg^{2+} ions facilitates the reduction of CO_2 in the whole potential range, and a shift in LSVs toward less negative potentials is observed. CO_2 adsorption on the surface of electrocatalysts, in our case, cobalt nodes, is an essential step in the CO_2 reduction mechanism [89,90]. Because of its important role in reducing efficiency, this step is considered a descriptor for CO_2 reduction. By adsorption of CO_2 on the surface and formation of chemisorption bond, the hybrid of central carbon changes from *sp* to sp^2. It means the bond angle should be reduced to angles smaller than 180°, which is too hard. It has been reported that Mg^{2+} ions can form a complex with adsorbed CO_2, in which the interaction between Mg^{2+} ions and oxygen atoms of CO_2 makes this bond bending more facile [35–37]. We suggest the same mechanism here works for the effects of Mg^{2+} ions in the solution for the adsorbed CO_2 molecules on the adsorbed cobalt nodes.

Finally, it should be noted that the effects of Mg^{2+} ion complex formation with adsorbed CO_2 molecules to facilitate CO_2 reduction for ZIF-67 NS are more observable than those for ZIF-67 NP, similar to the previous part of this work. Again, it could be related to the greater contribution of under–coordinated cobalt nodes and the facile traveling of CO_2 and Mg^{2+} ions into the layered structured ZIF-67 NS compared to ZIF-67 NP.

4. Conclusions

In summary, ZIF-67 nanoparticles and ZIF-67 nanosheets were successfully constructed by co–precipitation and one–pot hydrothermal method, respectively. The crystallinities, morphologies, and surface areas of the synthesized samples were confirmed by XRD, FE–SEM, and BET, respectively, and investigated toward CO_2 reduction as electrocatalysts. The ZIF-67 nanosheet exhibits better electrocatalytic activity compared to the ZIF-67 nanoparticle for CO_2 reduction. Such behavior was related to the significant contribution of under–coordinated cobalt nodes in the ZIF-67 nanosheet. Also, the existence of Mg^{2+} ions as Lewis acid cations promoted the CO_2 reduction reaction, suggesting the formation of the ZIF-67-CO_2-Mg^{2+} complex.

CRediT authorship contribution statement

Neda Sadat Barekati: Writing – original draft, Resources, Formal analysis, Data curation. **Hossein Farsi:** Writing – review & editing, Supervision, Conceptualization. **Alireza Farrokhi:** Methodology. **Shokufeh Moghiminia:** Validation, Methodology, Conceptualization.

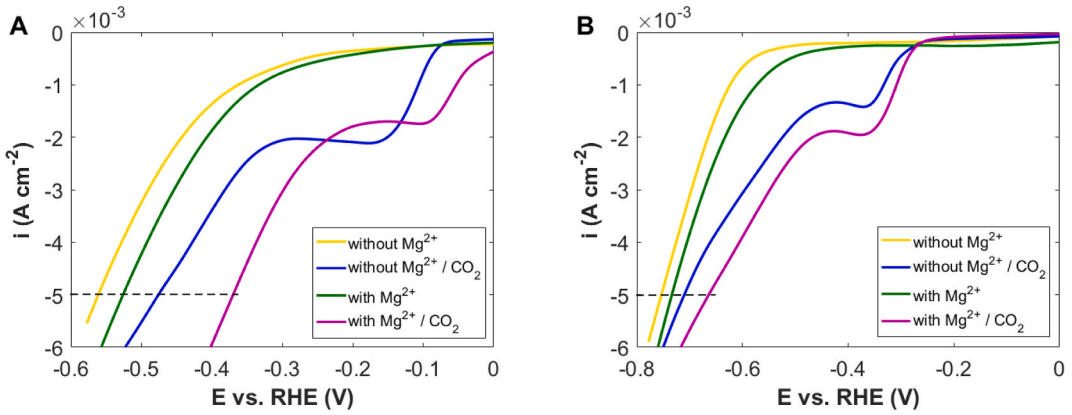

Fig. 7. LSVs for (A) ZIF-67 NS and (B) ZIF-67 NP in the 0.1 M $NaHCO_3$ + 0.1 M NaCl electrolyte and 0.1 M $NaHCO_3$ + 0.05 M $MgCl_2$ electrolyte with and without CO_2 bubbling.

Declaration of competing interest

The authors declare that they have no known competing financial interests or personal relationships that could have appeared to influence the work reported in this paper.

Appendix A. Supplementary data

Supplementary data to this article can be found online at https://doi.org/10.1016/j.heliyon.2024.e26281.

References

[1] G.A. Olah, G.K.S. Prakash, A. Goeppert, Anthropogenic chemical carbon cycle for a sustainable future, J. Am. Chem. Soc. 133 (2011) 12881–12898, https://doi.org/10.1021/ja202642y.
[2] H.Z. Wu, S. Bandaru, J. Liu, L.L. Li, L. Jin, Mechanism of CO_2 conversion into methanol and methane at the edge of graphitic carbon nitride sheet: a first-principle study, Carbon N. Y. 169 (2020) 73–81, https://doi.org/10.1016/j.carbon.2020.07.006.
[3] H. Zhao, Y. Lei, 3D nanostructures for the next generation of high-performance nanodevices for electrochemical energy conversion and storage, Adv. Energy Mater. 10 (2020), https://doi.org/10.1002/aenm.202001460.
[4] E.V. Kondratenko, G. Mul, J. Baltrusaitis, G.O. Larrazábal, J. Pérez-Ramírez, Status and perspectives of CO_2 conversion into fuels and chemicals by catalytic, photocatalytic and electrocatalytic processes, Energy Environ. Sci. 6 (2013) 3112–3135, https://doi.org/10.1039/c3ee41272e.
[5] X. Zhi, Y. Jiao, Y. Zheng, A. Vasileff, S.Z. Qiao, Selectivity roadmap for electrochemical CO_2 reduction on copper-based alloy catalysts, Nano Energy 71 (2020), https://doi.org/10.1016/j.nanoen.2020.104601.
[6] Y. Wang, C. Niu, D. Wang, Metallic nanocatalysts for electrochemical CO_2 reduction in aqueous solutions, J. Colloid Interface Sci. 527 (2018) 95–106, https://doi.org/10.1016/j.jcis.2018.05.041.
[7] F. Pan, W. Deng, C. Justiniano, Y. Li, Identification of champion transition metals centers in metal and nitrogen-codoped carbon catalysts for CO_2 reduction, Appl. Catal. B Environ. 226 (2018) 463–472, https://doi.org/10.1016/j.apcatb.2018.01.001.
[8] S. Lin, C.S. Diercks, Y.B. Zhang, N. Kornienko, E.M. Nichols, Y. Zhao, A.R. Paris, D. Kim, P. Yang, O.M. Yaghi, C.J. Chang, Covalent organic frameworks comprising cobalt porphyrins for catalytic CO2 reduction in water, Science 349 (2015) 1208–1213, https://doi.org/10.1126/science.aac8343 (80-.).
[9] A.S. Varela, N. Ranjbar Sahraie, J. Steinberg, W. Ju, H.S. Oh, P. Strasser, Metal-Doped nitrogenated carbon as an efficient catalyst for direct CO_2 electroreduction to CO and hydrocarbons, Angew. Chem. Int. Ed. 54 (2015) 10758–10762, https://doi.org/10.1002/anie.201502099.
[10] H. Furukawa, K.E. Cordova, M. O'Keeffe, O.M. Yaghi, The chemistry and applications of metal-organic frameworks, Science 341 (2013), https://doi.org/10.1126/science.1230444, 80-.
[11] E. Irandoost, H. Farsi, A. Farrokhi, Effects of water content on electrochemical capacitive behavior of nanostructured $Cu_3(BTC)_2$ MOF prepared in aqueous solution, Electrochim. Acta 368 (2021), https://doi.org/10.1016/j.electacta.2020.137616.
[12] J.B. Tan, G.R. Li, Recent progress on metal-organic frameworks and their derived materials for electrocatalytic water splitting, J. Mater. Chem. A 8 (2020) 14326–14355, https://doi.org/10.1039/d0ta04016a.
[13] W.W. Yuan, J.X. Wu, X. Da Zhang, S.Z. Hou, M. Xu, Z.Y. Gu, In situ transformation of bismuth metal-organic frameworks for efficient selective electroreduction of CO_2 to formate, J. Mater. Chem. A 8 (2020) 24486–24492, https://doi.org/10.1039/d0ta08092f.
[14] Q. Yang, Q. Xu, H.L. Jiang, Metal-organic frameworks meet metal nanoparticles: synergistic effect for enhanced catalysis, Chem. Soc. Rev. 46 (2017) 4774–4808, https://doi.org/10.1039/c6cs00724d.
[15] X. Yang, J. Pan, B. Xing, Z. Xie, Y. Fu, K. Cheng, Novel ZnO@NPC core–shell polyhedral heterostructures derived from ZIF-8 with enhanced photocatalytic performance for aflatoxin B1 degradation, Arab. J. Chem. 16 (2023), https://doi.org/10.1016/j.arabjc.2023.104789.
[16] X. Yang, J. Pan, J. Hu, S. Zhao, K. Cheng, MOF-derived La–$ZnFe_2O_4$@Fe_3O_4@carbon magnetic hybrid composite as a highly efficient and recyclable photocatalyst for mycotoxins degradation, Chem. Eng. J. 467 (2023), https://doi.org/10.1016/j.cej.2023.143381.
[17] X. Yang, J. Pan, B. Xing, W. Lei, Y. Fu, K. Cheng, Construction of a La-$ZnIn_2S_4$/MIL-125(Ti) heterojunction for highly efficient photocatalytic degradation of aflatoxin B1, Mater. Adv. 4 (2023) 940–947, https://doi.org/10.1039/d2ma01028c.
[18] B. You, N. Jiang, M. Sheng, W.S. Drisdell, J. Yano, Y. Sun, Bimetal-organic framework self-adjusted synthesis of support-free nonprecious electrocatalysts for efficient oxygen reduction, ACS Catal. 5 (2015) 7068–7076, https://doi.org/10.1021/acscatal.5b02325.
[19] X. Zhang, Y. Zhang, Q. Li, X. Zhou, Q. Li, J. Yi, Y. Liu, J. Zhang, Highly efficient and durable aqueous electrocatalytic reduction of CO_2 to HCOOH with a novel bismuth-MOF: experimental and DFT studies, J. Mater. Chem. A 8 (2020) 9776–9787, https://doi.org/10.1039/d0ta00384k.

[20] E. Irandoost, N.S. Barekati, H. Farsi, A. Farrokhi, G. Horvath, Z. Li, Cobalt–organic framework as a Bi–functional electrocatalyst for renewable hydrogen production by electrochemical water splitting, Appl. Energy Combust. Sci. (2023) 100240, https://doi.org/10.1016/j.jaecs.2023.100240.

[21] H. Wang, Q.L. Zhu, R. Zou, Q. Xu, Metal-organic frameworks for energy applications, Chem 2 (2017) 52–80, https://doi.org/10.1016/j.chempr.2016.12.002.

[22] J. Jiang, L. Huang, X. Liu, L. Ai, Bioinspired cobalt-citrate metal-organic framework as an efficient electrocatalyst for water oxidation, ACS Appl. Mater. Interfaces 9 (2017) 7193–7201, https://doi.org/10.1021/acsami.6b16534.

[23] A. Mahmood, W. Guo, H. Tabassum, R. Zou, Metal-organic framework-based nanomaterials for electrocatalysis, Adv. Energy Mater. 6 (2016), https://doi.org/10.1002/aenm.201600423.

[24] H. Jin, C. Guo, X. Liu, J. Liu, A. Vasileff, Y. Jiao, Y. Zheng, S.Z. Qiao, Emerging two-dimensional nanomaterials for electrocatalysis, Chem. Rev. 118 (2018) 6337–6408, https://doi.org/10.1021/acs.chemrev.7b00689.

[25] X. Chia, M. Pumera, Characteristics and performance of two-dimensional materials for electrocatalysis, Nat. Catal. 1 (2018) 909–921, https://doi.org/10.1038/s41929-018-0181-7.

[26] H. Wang, X. Liu, P. Niu, S. Wang, J. Shi, L. Li, Porous two-dimensional materials for photocatalytic and electrocatalytic applications, Matter 2 (2020) 1377–1413, https://doi.org/10.1016/j.matt.2020.04.002.

[27] H. Wu, J. Wang, W. Jin, Z. Wu, Recent development of two-dimensional metal-organic framework derived electrocatalysts for hydrogen and oxygen electrocatalysis, Nanoscale 12 (2020) 18497–18522, https://doi.org/10.1039/d0nr04458j.

[28] E. Irandoost, N.S. Barekati, H. Farsi, A. Farrokhi, S. Moghiminia, Ultrathin two-dimensional cobalt-organic framework nanosheets as an effective electrocatalyst for overall water splitting under alkaline conditions, Electrochim. Acta 466 (2023), https://doi.org/10.1016/j.electacta.2023.143075.

[29] K.S. Novoselov, et al., Electric field effect in atomically, Thin Carbon Films 306 (2016) 666–669.

[30] J. Wang, N. Li, Y. Xu, H. Pang, Two-dimensional MOF and COF nanosheets: synthesis and applications in electrochemistry, Chem. Eur J. 26 (2020) 6402–6422, https://doi.org/10.1002/chem.202000294.

[31] J.X. Wu, W.W. Yuan, M. Xu, Z.Y. Gu, Ultrathin 2D nickel zeolitic imidazolate framework nanosheets for electrocatalytic reduction of CO_2, Chem. Commun. 55 (2019) 11634–11637, https://doi.org/10.1039/c9cc05487a.

[32] X. Da Zhang, S.Z. Hou, J.X. Wu, Z.Y. Gu, Two-dimensional metal–organic framework nanosheets with cobalt-porphyrins for high-performance CO_2 electroreduction, Chem. Eur J. 26 (2020) 1604–1611, https://doi.org/10.1002/chem.201904072.

[33] A.R. Portis, H.W. Heldt, Light-dependent changes of the Mg^{2+} concentration in the stroma in relation to the Mg^{2+} dependency of CO_2 fixation in intact chloroplasts, BBA - Bioenerg. 449 (1976) 434–446, https://doi.org/10.1016/0005-2728(76)90154-7.

[34] A. Gardemann, D. Schimkat, H.W. Heldt, Control of CO_2 fixation regulation of stromal fructose-1,6-bisphosphatase in spinach by pH and Mg^{2+} concentration, Planta 168 (1986) 536–545, https://doi.org/10.1007/BF00392274.

[35] Y.Q. Wang, X.H. Dan, X. Wang, Z.Y. Yi, J. Fu, Y.C. Feng, J.S. Hu, D. Wang, L.J. Wan, Probing the synergistic effects of Mg^{2+} on CO_2 reduction reaction on CoPc by in situ electrochemical scanning tunneling microscopy, J. Am. Chem. Soc. 144 (2022) 20126–20133, https://doi.org/10.1021/jacs.2c09862.

[36] M. Hammouche, D. Lexa, J.M. Savêant, M. Momenteau, Chemical catalysis of electrochemical reactions. Homogeneous catalysis of the electrochemical reduction of carbon dioxide by Iron("0") porphyrins. Role of the addition of magnesium cations, J. Am. Chem. Soc. 113 (1991) 8455–8466, https://doi.org/10.1021/ja00022a038.

[37] I. Bhugun, D. Lexa, J.M. Savéant, Catalysis of the electrochemical reduction of carbon dioxide by iron(0) porphyrins. Synergistic effect of Lewis acid cations, J. Phys. Chem. 100 (1996) 19981–19985, https://doi.org/10.1021/jp9618486.

[38] D.A. Yang, H.Y. Cho, J. Kim, S.T. Yang, W.S. Ahn, CO_2 capture and conversion using Mg-MOF-74 prepared by a sonochemical method, Energy Environ. Sci. 5 (2012) 6465–6473, https://doi.org/10.1039/c1ee02234b.

[39] R. Das, S.S. Manna, B. Pathak, C.M. Nagaraja, Strategic design of Mg-centered porphyrin metal-organic framework for efficient visible light-promoted fixation of CO_2 under ambient conditions: combined experimental and theoretical investigation, ACS Appl. Mater. Interfaces (2022), https://doi.org/10.1021/acsami.2c07969.

[40] E. Andres-Garcia, L. Oar-Arteta, J. Gascon, F. Kapteijn, ZIF-67 as silver-bullet in adsorptive propane/propylene separation, Chem. Eng. J. 360 (2019) 10–14, https://doi.org/10.1016/j.cej.2018.11.118.

[41] R. Banerjee, A. Phan, B. Wang, C. Knobler, H. Furukawa, M. O'Keeffe, O.M. Yaghi, High-throughput synthesis of zeolitic imidazolate frameworks and application to CO_2 capture, Science 319 (2008) 939–943, https://doi.org/10.1126/science.1152516, 80-.

[42] M.H. Miles, Electrochemical reduction of carbon dioxide, TMS Annu. Meet. (2008) 129–133, https://doi.org/10.1149/2.030309jes.

[43] X. Peng, X. Jin, B. Gao, Z. Liu, P.K. Chu, Strategies to improve cobalt-based electrocatalysts for electrochemical water splitting, J. Catal. 398 (2021) 54–66, https://doi.org/10.1016/j.jcat.2021.04.003.

[44] E. Irandoost, H. Farsi, A. Farrokhi, N.S. Barekati, Z. Li, Environmentally benign synthesis of copper benzenetricarboxylic acid MOF as an electrocatalyst for overall water splitting and CO_2 reduction, ECS Adv 1 (2022) 020501, https://doi.org/10.1149/2754-2734/ac6ad5.

[45] H. Farsi, S. Moghiminia, M. Raygan, E. Dana, S. Hosseini, M. Behforooz, T. Zubkov, I.V. Lightcap, Z. Li, Nanostructured tungstate-derived copper for hydrogen evolution reaction and electroreduction of CO_2 in sodium hydroxide solutions, J. Phys. Chem. C 123 (2019) 25941–25948, https://doi.org/10.1021/acs.jpcc.9b07133.

[46] H. Farsi, E. Irandoost, N.S. Barekati, S. Moghiminia, S. Hosseini, T. Zubkov, J. Estes, L. Dumpert, I.V. Lightcap, Z. Li, Nanostructured $MnWO_4$ as a bifunctional electrocatalyst for water splitting, ECS J. Solid State Sci. Technol. 12 (2023) 083007, https://doi.org/10.1149/2162-8777/acec0d.

[47] H.T. Kwon, H.K. Jeong, A.S. Lee, H.S. An, J.S. Lee, Heteroepitaxially grown zeolitic imidazolate framework membranes with unprecedented propylene/propane separation performances, J. Am. Chem. Soc. 137 (2015) 12304–12311, https://doi.org/10.1021/jacs.5b06730.

[48] G. Lu, S. Li, Z. Guo, O.K. Farha, B.G. Hauser, X. Qi, Y. Wang, X. Wang, S. Han, X. Liu, J.S. Duchene, H. Zhang, Q. Zhang, X. Chen, J. Ma, S.C.J. Loo, W.D. Wei, Y. Yang, J.T. Hupp, F. Huo, Imparting functionality to a metal-organic framework material by controlled nanoparticle encapsulation, Nat. Chem. 4 (2012) 310–316, https://doi.org/10.1038/nchem.1272.

[49] Z. Li, X. Huang, C. Sun, X. Chen, J. Hu, A. Stein, B. Tang, Thin-film electrode based on zeolitic imidazolate frameworks (ZIF-8 and ZIF-67) with ultra-stable performance as a lithium-ion battery anode, J. Mater. Sci. 52 (2017) 3979–3991, https://doi.org/10.1007/s10853-016-0660-7.

[50] K.A. Cychosz, M. Thommes, Progress in the physisorption characterization of nanoporous gas storage materials, Engineering 4 (2018) 559–566, https://doi.org/10.1016/j.eng.2018.06.001.

[51] A. Dhakshinamoorthy, A.M. Asiri, H. Garcia, 2D metal–organic frameworks as multifunctional materials in heterogeneous catalysis and electro/photocatalysis, Adv. Mater. 31 (2019), https://doi.org/10.1002/adma.201900617.

[52] S. Moghiminia, H. Farsi, T. Zubkov, S. Hosseini, M. Behforouz, F. Fahmideh Mahdizadeh, N.S. Barekati, N.G. Moghadam, E. Irandoost, J. Estes, Z. Li, Revealing electronic structure of nanostructured cobalt titanate via a combination of optical and electrochemical approaches toward water splitting and CO_2 reduction, J. Chem. Technol. Biotechnol. 98 (2023) 2257–2265, https://doi.org/10.1002/jctb.7450.

[53] Y.J. Zhang, V. Sethuraman, R. Michalsky, A.A. Peterson, Competition between CO_2 reduction and H_2 evolution on transition-metal electrocatalysts, ACS Catal. 4 (2014) 3742–3748, https://doi.org/10.1021/cs5012298.

[54] X. Guo, M. Duan, J. Zhang, B. Xi, M. Li, R. Yin, X. Zheng, Y. Liu, F. Cao, X. An, S. Xiong, A general self-assembly induced strategy for synthesizing 2D ultrathin cobalt-based compounds toward optimizing hydrogen evolution catalysis, Adv. Funct. Mater. 32 (2022), https://doi.org/10.1002/adfm.202209397.

[55] L. Cao, Q. Luo, W. Liu, Y. Lin, X. Liu, Y. Cao, W. Zhang, Y. Wu, J. Yang, T. Yao, S. Wei, Identification of single-atom active sites in carbon-based cobalt catalysts during electrocatalytic hydrogen evolution, Nat. Catal. 2 (2019) 134–141, https://doi.org/10.1038/s41929-018-0203-5.

[56] T. Yang, H. Xie, N. Ma, E. Liu, C. Shi, C. He, N. Zhao, Unraveling the mechanism of hydrogen evolution reaction on cobalt compound electrocatalysts, Appl. Surf. Sci. 550 (2021), https://doi.org/10.1016/j.apsusc.2021.149355.

[57] R. Sun, X. Huang, J. Jiang, W. Xu, S. Zhou, Y. Wei, M. Li, Y. Chen, S. Han, Recent advances in cobalt-based catalysts for efficient electrochemical hydrogen evolution: a review, Dalt. Trans. 51 (2022) 15205–15226, https://doi.org/10.1039/d2dt02189g.

[58] M. Usman, M. Humayun, M.D. Garba, L. Ullah, Z. Zeb, A. Helal, M.H. Suliman, B.Y. Alfaifi, N. Iqbal, M. Abdinejad, A.A. Tahir, H. Ullah, Electrochemical reduction of CO_2: a review of cobalt based catalysts for carbon dioxide conversion to fuels, Nanomaterials 11 (2021), https://doi.org/10.3390/nano11082029.

[59] A. Chapovetsky, M. Welborn, J.M. Luna, R. Haiges, T.F. Miller, S.C. Marinescu, Pendant hydrogen-bond donors in cobalt catalysts independently enhance CO_2 reduction, ACS Cent. Sci. 4 (2018) 397–404, https://doi.org/10.1021/acscentsci.7b00607.

[60] C. Li, X. Tong, P. Yu, W. Du, J. Wu, H. Rao, Z.M. Wang, Carbon dioxide photo/electroreduction with cobalt, J. Mater. Chem. A 7 (2019) 16622–16642, https://doi.org/10.1039/c9ta03892b.

[61] H. Zhong, K. Fujii, Y. Nakano, F. Jin, Effect of CO_2 bubbling into aqueous solutions used for electrochemical reduction of CO_2 for energy conversion and storage, J. Phys. Chem. C 119 (2015) 55–61, https://doi.org/10.1021/jp509043h.

[62] J.S. Zeng, N. Corbin, K. Williams, K. Manthiram, Kinetic analysis on the role of bicarbonate in carbon dioxide electroreduction at immobilized cobalt phthalocyanine, ACS Catal. 10 (2020) 4326–4336, https://doi.org/10.1021/acscatal.9b05272.

[63] H. Ooka, M.C. Figueiredo, M.T.M. Koper, Competition between hydrogen evolution and carbon dioxide reduction on copper electrodes in mildly acidic media, Langmuir 33 (2017) 9307–9313, https://doi.org/10.1021/acs.langmuir.7b00696.

[64] W. Sheng, M. Myint, J.G. Chen, Y. Yan, Correlating the hydrogen evolution reaction activity in alkaline electrolytes with the hydrogen binding energy on monometallic surfaces, Energy Environ. Sci. 6 (2013) 1509–1512, https://doi.org/10.1039/c3ee00045a.

[65] S. Abner, A. Chen, Design and mechanistic study of advanced cobalt-based nanostructured catalysts for electrochemical carbon dioxide reduction, Appl. Catal. B Environ. 301 (2022), https://doi.org/10.1016/j.apcatb.2021.120761.

[66] Z. Pan, N. Pan, L. Chen, J. He, M. Zhang, Flower-like MOF-derived Co–N-doped carbon composite with remarkable activity and durability for electrochemical hydrogen evolution reaction, Int. J. Hydrogen Energy 44 (2019) 30075–30083, https://doi.org/10.1016/j.ijhydene.2019.09.117.

[67] L. Fan, Z. Kang, M. Li, D. Sun, Recent progress in pristine MOF-based catalysts for electrochemical hydrogen evolution, oxygen evolution and oxygen reduction, Dalt. Trans. 50 (2021) 5732–5753, https://doi.org/10.1039/d1dt00302j.

[68] B.B. Beyene, S.B. Mane, C.-H. Hung, Electrochemical hydrogen evolution by cobalt (II) porphyrins: effects of ligand modification on catalytic activity, efficiency and overpotential, J. Electrochem. Soc. 165 (2018) H481–H487, https://doi.org/10.1149/2.0481809jes.

[69] I. Hod, P. Deria, W. Bury, J.E. Mondloch, C.W. Kung, M. So, M.D. Sampson, A.W. Peters, C.P. Kubiak, O.K. Farha, J.T. Hupp, A porous proton-relaying metal-organic framework material that accelerates electrochemical hydrogen evolution, Nat. Commun. 6 (2015), https://doi.org/10.1038/ncomms9304.

[70] N. Mahmood, Y. Yao, J.W. Zhang, L. Pan, X. Zhang, J.J. Zou, Electrocatalysts for hydrogen evolution in alkaline electrolytes: mechanisms, challenges, and prospective solutions, Adv. Sci. 5 (2018), https://doi.org/10.1002/advs.201700464.

[71] C.W. Lee, N.H. Cho, S.W. Im, M.S. Jee, Y.J. Hwang, B.K. Min, K.T. Nam, New challenges of electrokinetic studies in investigating the reaction mechanism of electrochemical CO_2 reduction, J. Mater. Chem. A 6 (2018) 14043–14057, https://doi.org/10.1039/c8ta03480j.

[72] M. Dunwell, W. Luc, Y. Yan, F. Jiao, B. Xu, Understanding surface-mediated electrochemical reactions: CO_2 reduction and beyond, ACS Catal. 8 (2018) 8121–8129, https://doi.org/10.1021/acscatal.8b02181.

[73] A. Wuttig, M. Yaguchi, K. Motobayashi, M. Osawa, Y. Surendranath, Inhibited proton transfer enhances Au-catalyzed CO_2-to-fuels selectivity, Proc. Natl. Acad. Sci. U. S. A. 113 (2016) E4585–E4593, https://doi.org/10.1073/pnas.1602984113.

[74] D.H. Won, C.H. Choi, J. Chung, M.W. Chung, E.H. Kim, S.I. Woo, Rational design of a hierarchical tin dendrite electrode for efficient electrochemical reduction of CO_2, ChemSusChem 8 (2015) 3092–3098, https://doi.org/10.1002/cssc.201500694.

[75] C. Rogers, W.S. Perkins, G. Veber, T.E. Williams, R.R. Cloke, F.R. Fischer, Synergistic enhancement of electrocatalytic CO_2 reduction with gold nanoparticles embedded in functional graphene nanoribbon composite electrodes, J. Am. Chem. Soc. 139 (2017) 4052–4061, https://doi.org/10.1021/jacs.6b12217.

[76] C. Kim, H.S. Jeon, T. Eom, M.S. Jee, H. Kim, C.M. Friend, B.K. Min, Y.J. Hwang, Achieving selective and efficient electrocatalytic activity for CO_2 reduction using immobilized silver nanoparticles, J. Am. Chem. Soc. 137 (2015) 13844–13850, https://doi.org/10.1021/jacs.5b06568.

[77] Y. Song, R. Peng, D.K. Hensley, P.V. Bonnesen, L. Liang, Z. Wu, H.M. Meyer, M. Chi, C. Ma, B.G. Sumpter, A.J. Rondinone, High-selectivity electrochemical conversion of CO_2 to ethanol using a copper nanoparticle/N-doped graphene electrode, ChemistrySelect 1 (2016) 6055–6061, https://doi.org/10.1002/slct.201601169.

[78] Z. Cao, D. Kim, D. Hong, Y. Yu, J. Xu, S. Lin, X. Wen, E.M. Nichols, K. Jeong, J.A. Reimer, P. Yang, C.J. Chang, A molecular surface functionalization approach to tuning nanoparticle electrocatalysts for carbon dioxide reduction, J. Am. Chem. Soc. 138 (2016) 8120–8125, https://doi.org/10.1021/jacs.6b02878.

[79] M. Ma, B.J. Trześniewski, J. Xie, W.A. Smith, Selective and efficient reduction of carbon dioxide to carbon monoxide on oxide-derived nanostructured silver electrocatalysts, Angew. Chemie. 128 (2016) 9900–9904, https://doi.org/10.1002/ange.201604654.

[80] Z. Chang, S. Huo, W. Zhang, J. Fang, H. Wang, Te tunable and highly selective reduction products on Ag@Cu bimetallic catalysts toward CO_2 electrochemical reduction reaction, J. Phys. Chem. C 121 (2017) 11368–11379, https://doi.org/10.1021/acs.jpcc.7b01586.

[81] Y. Chen, M.W. Kanan, Tin oxide dependence of the CO_2 reduction efficiency on tin electrodes and enhanced activity for tin/tin oxide thin-film catalysts, J. Am. Chem. Soc. 134 (2012) 1986–1989, https://doi.org/10.1021/ja2108799.

[82] F. Li, L. Chen, G.P. Knowles, D.R. MacFarlane, J. Zhang, Hierarchical mesoporous SnO_2 nanosheets on carbon cloth: a robust and flexible electrocatalyst for CO_2 reduction with high efficiency and selectivity, Angew. Chemie. 129 (2017) 520–524, https://doi.org/10.1002/ange.201608279.

[83] S. Gao, X. Jiao, Z. Sun, W. Zhang, Y. Sun, C. Wang, Q. Hu, X. Zu, F. Yang, S. Yang, L. Liang, J. Wu, Y. Xie, Ultrathin Co_3O_4 layers realizing optimized CO_2 electroreduction to formate, Angew. Chem. Int. Ed. 55 (2016) 698–702, https://doi.org/10.1002/anie.201509800.

[84] H. Gu, G. Shi, L. Zhong, L. Liu, H. Zhang, C. Yang, K. Yu, C. Zhu, J. Li, S. Zhang, C. Chen, Y. Han, S. Li, L. Zhang, A two-dimensional van der Waals heterostructure with isolated electron-deficient cobalt sites toward high-efficiency CO_2 electroreduction, J. Am. Chem. Soc. 144 (2022) 21502–21511, https://doi.org/10.1021/jacs.2c07601.

[85] Y. Song, J.J. Zhang, Y. Dou, Z. Zhu, J. Su, L. Huang, W. Guo, X. Cao, L. Cheng, Z. Zhu, Z. Zhang, X. Zhong, D. Yang, Z. Wang, B.Z. Tang, B.I. Yakobson, R. Ye, Atomically thin, ionic–covalent organic nanosheets for stable, high-performance carbon dioxide electroreduction, Adv. Mater. 34 (2022), https://doi.org/10.1002/adma.202110496.

[86] T. Yuan, T. Wang, G. Zhang, W. Deng, D. Cheng, H. Gao, J. Zhao, J. Yu, P. Zhang, J. Gong, The effect of specific adsorption of halide ions on electrochemical CO_2 reduction, Chem. Sci. 13 (2022) 8117–8123, https://doi.org/10.1039/d2sc02689a.

[87] Y. Hori, A. Murata, R. Takahashi, Formation of hydrocarbons in the electrochemical reduction of carbon dioxide at a copper electrode in aqueous solution, J. Chem. Soc. Faraday Trans. 1 Phys. Chem. Condens. Phases. 85 (1989) 2309–2326, https://doi.org/10.1039/F19898502309.

[88] Y. Huang, C.W. Ong, B.S. Yeo, Effects of electrolyte anions on the reduction of carbon dioxide to ethylene and ethanol on copper (100) and (111) surfaces, ChemSusChem 11 (2018) 3299–3306, https://doi.org/10.1002/cssc.201801078.

[89] J. Schneider, H. Jia, J.T. Muckerman, E. Fujita, Thermodynamics and kinetics of CO_2, CO, and H^+ binding to the metal centre of CO_2 reduction catalysts, Chem. Soc. Rev. 41 (2012) 2036–2051, https://doi.org/10.1039/c1cs15278e.

[90] M. Loipersberger, D.Z. Zee, J.A. Panetier, C.J. Chang, J.R. Long, M. Head-Gordon, Computational study of an iron(II) polypyridine electrocatalyst for CO_2 reduction: key roles for intramolecular interactions in CO_2 binding and proton transfer, Inorg. Chem. 59 (2020) 8146–8160, https://doi.org/10.1021/acs.inorgchem.0c00454.